Dynamical coupling between the low-latitude lower thermosphere and ionosphere via the non-migrating diurnal tide as revealed by concurrent satellite observations and numerical modeling

Federico Gasperini[1], Irfan Azeem[1], Geoff Crowley[1], Michael Perdue[2], Matthew Depew[2], Thomas Immel[3], Erik Stromberg[1], Chad Fish[1], Crystal Frazier[1], Adam Reynolds[1], Anthony Swenson[1], Ted Tash[1], Russell Gleason[1], Ryan Blay[1], Jordan Maxwell[1], Keith Underwood[1], Christian Frazier[1], Scott Jensen[1]

[1]Atmospheric and Space Technology Research Associates, 282 Century Pl #1000, Louisville, CO, USA
[2]William B. Hanson Center for Space Sciences, Physics Department, University of Texas at Dallas, Richardson, TX, USA
[3]Space Sciences Laboratory, University of California, Berkeley, CA, USA

Key Points:

- A large-amplitude zonal wavenumber 4 (WN4) structure in the low-latitude ionosphere-thermosphere (IT) is seen in multiple satellite observations
- Numerical simulations demonstrate the non-migrating diurnal tide DE3 to be responsible for this strong IT WN4 coupling
- SORTIE and ICON IVM observations provide useful insights into the influence of tropical tropospheric deep convection on IT variability

Corresponding author: Federico Gasperini, `fgasperini@astraspace.net`

Abstract

The diurnal-eastward propagating tide with zonal wavenumber 3 (DE3) has gained significant attention due to its ability to preferentially propagate to the ionosphere and thermosphere (IT) from the tropical troposphere, thus effectively coupling these atmospheric regions. In this work, we demonstrate the existence of a pronounced zonal wavenumber 4 (WN4) structure in the low-latitude ionosphere during May 27 - June 5, 2020 using concurrent in-situ total ion number density measurements from the Scintillation Observations and Response of The Ionosphere to Electrodynamics (SORTIE) and the Ionospheric Connection Explorer (ICON) satellites. Temperature observations from the Thermosphere Ionosphere Mesosphere Energetics Dynamics Sounding of the Atmosphere using Broadband Emission Radiometry (TIMED/SABER) instrument near 105 km and output from the Specified Dynamics Whole Atmosphere Community Climate Model with thermosphere and ionosphere eXtension (SD/WACCM-X) demonstrate that this global-scale ionospheric WN4 structure is due to DE3 propagating through the lower thermosphere.

Plain Language Summary

The extent to which terrestrial weather (below ∼30 km) can influence the ionosphere and thermosphere (IT) is a fascinating discovery of the last two decades or so. The IT is known to vary significantly from day to day, and this daytoday weather is largely driven by processes originating in the lower atmosphere, especially during periods of quiet solar activity. Accurate forecasting of the IT variability thus depends on the ability to forecast the component that originates in the lower atmosphere. Ionospheric variability translates to uncertainty in navigation and communications systems, while thermospheric variability translates to uncertainty in orbital and reentry predictions. In this work, we present evidence of a large amplitude structure with four longitudinally-distributed peaks in the lower thermosphere and ionosphere associated with the well-known diurnal-eastward propagating tide with zonal wavenumber 3 (DE3) originating in the tropical troposphere. This is accomplished by using concurrent SORTIE, ICON, and TIMED satellite observations during May 27 - June 5, 2020 and a whole atmosphere model. SORTIE and ICON prove to be excellent observational platforms for studying the influence of terrestrial weather on IT variability.

1 Introduction

The lower atmosphere drives variability in the ionosphere-thermosphere (IT) system through the vertical propagation of waves, including tides, planetary waves, and Kelvin waves. These waves are periodic in time and longitude due to the rotation of the Earth, and interact with the lower IT region to modulate electric fields that map to higher altitudes and redistribute plasma in the 200-1000 km region. Due to the geometry of magnetic field lines near the equator, much of this variability occurs at low latitudes and is driven by waves that are excited by deep convective processes in the tropical troposphere and that propagate upwards into the IT system. Tropical troposphere variability is essentially mapped to the IT system through a variety of neutral-plasma coupling processes, and over a range of spatial and temporal scales. One important class of global-scale atmospheric waves characterized by periods that are harmonics of a solar day are thermal tides. These atmospheric tides can be generated in different altitudinal regions due to tropospheric latent heating, absorption of tropospheric infrared radiation by water vapor, absorption of solar ultraviolet radiation by stratospheric ozone, thermosphere molecular oxygen absorption of extreme ultraviolet radiation, and wave-wave interactions (e.g., Chapman and Lindzen, 1970; Hagan and Forbes, 2002; Hagan et al., 2007; Liu, 2016). The main pathways responsible for the modulation of the ionosphere by tides are direct propagation of atmospheric tides into the ionosphere and thermosphere (e.g., Hagan et al., 2007; Oberheide et al., 2009) and indirect coupling via the ionosphere E-region dynamo (e.g., Jin et al., 2008; Ren et al., 2010; Wan et al., 2008, 2010, 2012).

Several studies investigated the importance of IT variability driven by lower-atmosphere wave sources. Initial work (e.g., Hagan et al., 2007; Jin et al., 2008; Fang et al., 2009; Wan et al., 2010) focused on verifying Sagawa et al.s (2005) and Immel et al.s (2006) suggestion that the wavenumber-4 (hereafter, WN4) structure seen in satellite-borne Sun-synchronous F-region ionospheric data was due to the modulation of dynamo electric fields by non-migrating tides propagating from below, and in particular due to the diurnal eastward-propagating tide with zonal wavenumber 3 (s = -3, i.e., DE3). DE3 originates in the tropical troposphere by latent heat release in deep convective clouds (e.g., Hagan, 1996; Hagan and Forbes, 2002, Lieberman et al., 2007), and its first equatorially-symmetric Hough mode is the largest component in the lower thermosphere (Oberheide et al., 2009; Truskowski et al., 2014), capable of propagating well into the middle thermosphere (Oberheide et al., 2011; Gasperini et al., 2015, 2017a, 2018) due to its longer vertical wavelength. When viewed at quasi-fixed local time (LT) from slowly precessing satellites, this feature manifests as a 4peak longitude structure. Subsequent studies examined the LT and seasonal variations of related WN4 and WN3 structures (e.g., Lin et al., 2007; Liu and Watanabe, 2008; Ren et al., 2009), and investigated the underlying mechanisms in further depth (e.g., Oberheide et al., 2011; He et al., 2011; Mukhtarov and Pancheva, 2011; Maute et al., 2012; Chang et al., 2013; Lei et al., 2014; Cho et al., 2015; Onohara et al., 2018).

In this work, we present observational evidence of prominent WN4 coupling between the lower thermosphere near 105 km and the ionospheric F-region at heights near 420 km and 590 km during May 27 - June 5, 2020. Our results take advantage of total ion number density (hereafter, ion density) measurements from the Ion Velocity Meter (IVM) instruments onboard the Scintillation Observations and Response of The Ionosphere to Electrodynamics (SORTIE) and Ionospheric Connection Explorer (ICON) spacecrafts and kinetic temperature observations from the Sounding of the Atmosphere using Broadband Emission Radiometry (SABER) instrument onboard the Thermosphere Ionosphere Mesosphere Energetics Dynamics (TIMED) satellite. We further connect this WN4 longitude variability to DE3 and investigate its latitude-height amplitude and phase structure using a Whole Atmosphere Community Climate Model with thermosphere and ionosphere eXtension (SD/WACCM-X) simulation with realistic wave forcing imposed by nudging Modern-Era Retrospective analysis for Research and Applications version-2 (MERRA-2) reanalysis data in the troposphere and stratosphere. After a brief description of the data, models, and methods (Section 2), we present in detail the observational and modeling results regarding the WN4 variability and its connection to the DE3 tide (Section 3), and conclude with a brief summary (Section 4).

2 Data, Models, and Methods

2.1 SORTIE/IVM

SORTIE is a NASA Heliophysics System Observatory (HSO) 6U CubeSat mission to investigate the underlying causes behind the appearance of plasma structures in the F-region ionosphere, leading to equatorial plasma bubbles, and the evolution of these structures after their formation (Crowley et al., 2016). SORTIE was launched onboard Dragon CRS-19 to the International Space Station (ISS), from where it was deployed on February 19, 2020 in a nearly circular orbit near 420 km with $\sim$51.6° inclination. It carries two science instruments, a miniature IVM (MIVM), and a micro-Planar Langmuir Probe (Crowley et al., 2016). This study employs SORTIE's IVM Level 2 ion density data product.

2.2 ICON/IVM

ICON is a NASA HSO mission designed to study the fundamental connections between the dynamics of the neutral atmosphere at altitudes between 100 km and 300 km and the charged particle motions at low and middle latitudes from a nearly circular orbit at an altitude near 590 km with ∼27° inclination (Immel et al., 2018). The ICON payload includes an IVM instrument that provides in situ measurements of the ion drift motions, density, temperature and major ion composition (Heelis et al., 2017). The IVM is comprised of two instruments, the Retarding Potential Analyzer (RPA) and the Drift Meter (DM). This study employs ICON's IVM-A Data Product 2.7 v4 determined from RPA measurements. Preliminary validation work by the ICON IVM team reports accuracy below $\pm 10^3$ cm^{-3} for this data product (see the acknowledgments for further information).

2.3 TIMED/SABER

The SABER instrument was launched onboard the TIMED satellite (also a NASA HSO mission) on December 7, 2001. SABER provides measurements of kinetic temperature from ∼20 km to ∼120 km altitude (Mertens et al., 2001). SABER views the atmospheric limb from an orbit of ∼625 km altitude and ∼73° inclination, so that the latitude coverage on a given day extends from about 53° in one hemisphere to about 83° in the other. This viewing geometry alternates once every ∼60 days. Errors in the retrieved temperatures in the 80-105 km region are estimated to be ±1.5-5 K (Garcia-Comas et al., 2008).

2.4 WACCM-X

WACCM-X (Liu et al., 2018) is a configuration of the National Center for Atmospheric Research (NCAR) Community Earth System Model (CESM) (Hurrell et al., 2013) that extends the atmospheric component into the thermosphere, with a model top boundary between 500 and 700 km. The standard spatial resolution of WACCM-X is 1.9° by

2.5° in latitude and longitude, respectively, and 1/4 scale height vertically above the upper stratosphere. To simulate the lower and middle atmosphere, WACCM-X can be run with specified dynamics (SD) that constrains the troposphere and stratosphere dynamics using MERRA-2 reanalysis data (Gelaro et al., 2017). This study employs output from an extended SD/WACCM-X version v2.1 simulation that covers the May 27 - June 5, 2020 period. The empirical ion convection patterns are specified using the Heelis et al. (1982) empirical model. The MERRA-2 forcing provides a realistic representation of the wave forcing in the lower and middle atmosphere making this simulation an ideal physics-based framework for interpreting atmosphere-ionosphere coupling by tides.

2.5 Analysis of Satellite Data

When combined, the ascending and descending nodes of SORTIE and ICON cover 24-hour of LT in ∼30 days (i.e., each node samples ∼4 hours of LT in about 10 days). Figure 1 shows the LT coverage of ICON (blue plus signs) and SORTIE (red squares) IVM measurements at 25°N (panel *b*), at the equator (panel *c*), and at 25°S (panel *d*) during May 27 - June 5, 2020. At the equator, SORTIE's (ICON's) orbit precesses from ∼2 LT/∼14 LT (∼7 LT/∼19 LT) on May 27 to ∼22 LT/∼10 LT (∼2 LT/∼14 LT) on June 5 (Figure 1*c*). As shown in Figure 1*a*, this 10-day period is characterized by low solar activity (average F10.7 ∼70) with two minor geomagnetic disturbances (ap∼25 on May 30, 2020 and ap∼15 on June 1-2, 2020). For this study, ICON and SORTIE IVM ion density are analyzed by both combining and separating ascending and descending node measurements. Wave analysis is performed by least-squares fitting SORTIE IVM ion density in 30-day sliding windows and 3-hourly SD/WACCM-X ion density and temperature during May 27 - June 5, 2020. Note that no least squares fitting of ICON data is performed here as this analysis is left for future work.

3 Results

The global distribution of ion density observed by SORTIE (ICON) IVM near 420 km (590 km) altitude during May 27 - June 5, 2020 is presented in Figure 2. SORTIE daytime (∼10-14 LT) and nighttime (∼22-2 LT) 10-day averages are shown in panels *a* and *b*, respectively. Figures 2a' and 2b' show the corresponding ICON daytime (∼14-18 LT) and nighttime (∼2-6 LT) 10-day averages, respectively. Excellent low-latitude coverage is achieved by both SORTIE (about ±51.6° latitude) and ICON (about ±27.1° latitude) during this 10-day period, as evidenced by the distribution of the black dots in panels a-a' and b-b' showing the measurement locations. Ion density values up to $\sim$4.4x10^5 cm^{-3} ($\sim$2.2x10^5 cm^{-3}) are observed during daytime and up to $\sim$1.7x10^5 cm^{-3} ($\sim$0.8x10^5 cm^{-3}) during nighttime by SORTIE (ICON) IVM. Note that a scaling factor is applied multiplying the ICON ion density by a factor of 2 given ICON's higher mean altitude (i.e., $\sim$590 km versus $\sim$420 km for SORTIE). Figures $2a''$-$2b''$ display ascending and descending node differences for SORTIE and ICON IVM ion density, respectively, each scaled (multiplied) by 0.5. Both SORTIE and ICON show enhanced ion density at low latitudes around 30°S-30°N with a prominent WN4 structure and peaks near 180°E, 100°E, 45°E, and 100°W. This type of feature in the low-latitude ionosphere was reported in previous satellite-based measurements (e.g., Immel et al., 2006; Lin et al., 2007; Liu and Watanabe, 2008, Liu et al., 2009), as discussed in Section 1. This notable WN4 structure observed by SORTIE and ICON points to a possible modulation of the background ion density by the non-migrating DE3 tide as observed from their slowly precessing orbits. Note that the equatorial ionization anomaly (EIA) is not evident in Figure 2 likely due SORTIE's and ICON's mean altitude ($\sim$420 km and $\sim$590 km, respectively) being significantly higher than the F-layer peak height ($\sim$200-350 km), in agreement with Figure 2 of Mukhtarov and Pancheva (2011).

It is important to realize that while the variability due to the semidiurnal eastward-propagating tide with s = -2 (SE2) and stationary planetary wave 4 (SPW4) would largely be eliminated by the ascending/descending node differences shown in Figures $2a''$-$2b''$, aliasing from the diurnal westward-propagating tide with s = 5 (DW5) and from the terdiurnal eastward-propagating tide with s = -1 (TE1) may also contribute to a WN4 longitude structure seen at a constant LT (see Lieberman, 1991; Oberheide et al., 2000; Gasperini et al., 2015, 2017b, 2018, 2020). Thus, to best investigate the origin of the observed WN4 structure we (1) combine 30 days of SORTIE data collected during May 27 - June 25, 2020 to acquire full 24-hour LT coverage, and (2) use output from a 3-hourly SD/WACCM-X simulation. Figure 3 shows the period versus zonal wavenumber amplitude spectra of SORTIE IVM ion density obtained by combining ascending and descending node measurements during May 27 - June 25, 2020 (panels a-a'') and SD/WACCM-X ion density during May 27 - June 5, 2020 derived using the full model output (panels b-b''). Around 10°S-10°N magnetic latitude (MLAT) both SORTIE (panels a') and WACCM-X (panel b') ion density spectra reveal the existence of a pronounced DE3 component with amplitudes of $\sim$2x10^4 cm^{-3}. DE3 is found to be nearly absent in both SORTIE and WACCM-X ion density at 40°N MLAT (panels a and b) and 40°S MLAT (panels a'' and b''), in agreement with the well-known Kelvin wave behavior of the first-symmetric equatorially-trapped Hough mode of DE3 that efficiently propagates to the IT. Also present in the spectra is the migrating DW1 tide, as shown in previous ionospheric observations (e.g., Chang et al., 2013). SW2, DW5 and TE1 amplitudes are found to be negligible (TE1 results not shown here), providing confidence to our assertion that the WN4 structure observed by SORTIE and ICON is in fact due to the non-migrating DE3 tide.

To examine the latitudinal structure associated with DE3 (and other diurnal tides), Figure 4 shows the MLAT-wavenumber diurnal amplitude spectra of SORTIE IVM (panels a and a') and SD/WACCM-X (panels b and b') ion densities with and without filtering the migrating DW1 tide. Similar to the results presented in Figure 3, SORTIE and WACCM-X show general agreement with large DW1 ($\sim$7x10^4 cm^{-3}) and DE3 ($\sim$3x10^4 cm^{-3}) amplitude variations primarily confined to low latitudes. Along with the pronounced DW1 and DE3, SORTIE spectra also exhibit D0 and DW2 variations (and some DE2), while WACCM-X spectra show DE1 and DW2 variations. Larger DE3 amplitudes (up to 3.06x10^4 cm^{-3}) are found around 25°N-10°S MLAT in the SORTIE spectra (panel 4a') consistent with the results shown in Figure 2a'', while WACCM-X maxima are found near 10°N-20°S MLAT. Some differences between the SORTIE and WACCM-X spectra are not unexpected and are likely due to (1) the different averaging window used (30 days for SORTIE and 10 day for WACCM-X; note that a 10-day window for WACCM-X is adopted for consistency with the SORTIE and ICON results shown in Figure 2), (2) differences in the longitude-local time sampling between model and observations, and (3) inherent tidal variability observed by SORTIE that is not reproduced by the model. Even with the amplitude suppression associated with the monthly averaging, panel 4a' shows SORTIE IVM ion density DE3 amplitudes exceeding $\sim$3x10^4 cm^{-3}, i.e, over 15% of the observed zonal mean.

Additional analysis of the DE3 tide in the ionosphere is performed using a 30-day sliding window of low-MLAT (±20°) SORTIE IVM ion density during the 4-month interval from May 27, 2020 through September 15, 2020 to investigate its temporal variability. Figure 5 show daily DE3 amplitudes (panel a) and phases (panel a') derived using a least squares method and the combined ascending/descending node data (i.e., covering $\sim$24-hr LT). DE3 amplitudes are found to be larger ($\sim$1.9x10^4 cm^{-3}) around May

27 - June 25, quickly decreasing to minima (10^3–10^4 cm^{-3}) near June - July, with largest amplitudes (∼2.1x10^4 cm^{-3}) observed during mid-August through early September 2020. The latitude structure of DE3 presented in Figure 4 and its temporal variation shown in Figure 5*a*, with largest amplitudes occurring around August-September and a second period of enhanced activity around April-May, is consistent with previous modeling work and observations (e.g., Mukhtarov and Pancheva, 2011; Truskowski et al., 2014; Gasperini et al., 2015). To investigate the altitude-latitude structure of the DE3 tide in the IT region, Figure 5*b* shows the SD/WACCM-X height (∼100-450 km) - MLAT (60°S-60°N) structure of ion density (panels b and b') and temperature (panels c and c') amplitudes and phases during May 27 - June 5, 2020. Ionospheric DE3 amplitudes are found to be largest around the F-layer peak near 200-350 km, with a defined 2-peak structure and maxima of ∼8x10^4 cm^{-3} around 15°N and 15°S associated with the EIA (Appleton, 1946; Balan and Bailey, 1995). Previous studies (e.g., Sagawa et al., 2005; Immel et al., 2006; Wan et al., 2008) showed the EIA to exhibit a WN4 longitudinal variation and it is now well accepted that this structure in the ionospheric F-region can form as a result of the combined effect of the E-region dynamo modulation by the lower thermospheric DE3 and from the direct propagation of DE3 into the F-region. It would be beyond the scope of this study to investigate the relative contribution of these two effects to the ionospheric DE3 observed by SORTIE and ICON and this effort is left for follow-on work. The lower thermospheric temperature DE3 exhibits largest amplitudes of ∼12 K around 110-120 km, in accord with previous modeling (e.g., Gasperini et al., 2015, 2017a) and observational (e.g., Truskowski et al., 2014) results. The vertical wavelength of the modeled temperature DE3 inferred from its vertical phase progression (panel c') is ∼49.8 km, in line with a predominant first symmetric Hough mode. Latitudinal asymmetries and broadening of the latitude structure with height in the thermospheric DE3 are likely due to the combined effect of mean winds and dissipation (e.g., Forbes, 2000; Gasperini et al., 2015, 2017a).

Figure 6 displays maps of TIMED/SABER temperatures near 105 km observed concurrently (i.e., May 27 - June 5, 2020) with the SORTIE and ICON IVM ion density maps presented in Figure 2. Panels a and b show results for the descending (∼3-5 LT) and ascending (∼15-17 LT) nodes, respectively; while panel c contains results for half ascending/descending node differences. A prominent WN4 structure is found to dominate the low-latitude (±30°) lower thermosphere with observed amplitude maxima of ∼30 K peaking near 135°E, 75°E, 45°W, 135°W. Pearson correlation coefficients between the equatorial WN4 structure in TIMED/SABER temperature and SORTIE (ICON) IVM ion density observations are calculated to be r=0.71 (r=0.66). This level of correlation, along with the modeling work discussed in Figure 5, provides strong evidence that the ionospheric WN4 structure observed by SORTIE and ICON is in fact associated with the lower thermospheric DE3. As noted earlier, a more comprehensive follow-on work (beyond the purview of the current investigation) will address the extent to which this DE3 signature observed in the ionospheric F-region is a result of the effect of the E-region dynamo modulation by the lower thermospheric DE3 versus the direct propagation of DE3 into the F-region.

4 Summary and Conclusions

Results presented above provide a clear picture of a marked longitudinal WN4 variation observed during May 27 - June 5, 2020 by SORTIE and ICON IVM in the low-latitude ionosphere near 420 km and 590 km, respectively. Taking advantage of output from an SD/WACCM-X simulation nudged with MERRA-2 reanalysis data in the troposphere and stratosphere and monthly-averaged SORTIE IVM data, we demonstrated that this prominent WN4 structure in the F-region ion density is due to the well-known DE3 tide. This non-migrating tide has gained significant attention due to its ability to preferentially propagate to the IT from the tropical troposphere, thus effectively coupling these atmospheric regions. SORTIE IVM observations and SD/WACCM-X output showed ion density DE3 amplitudes upward of 3x10^4 cm^{-3} (i.e., over 15% of the zonal mean) at low-latitudes (±20° MLAT), with general agreement between model and observations. Least-squares fitting of monthly-averaged SORTIE IVM ion density during May 27 - September 15, 2020 showed larger (∼1.9x10^4 cm^{-3}) DE3 amplitudes around May 27 - June 25, rapidly decreasing to smaller values (10^3−10^4 cm^{-3}) around June - July, and becoming largest (∼2.1x10^4 cm^{-3}) around mid-August through early September 2020, in agreement with the well-known seasonal variation of DE3 amplitudes found in previous modeling and observational studies (e.g., Mukhtarov and Pancheva, 2011; Truskowski et al., 2014; Gasperini et al., 2015, 2017a). Concurrent TIMED/SABER temperature observations near 105 km also showed a pronounced (±30 K) WN4 structure in the low-latitude lower thermosphere associated with DE3 that was found to be highly correlated with the ionospheric WN4 (r=0.71 for SABER/SORTIE and r=0.66 for SABER/ICON).

The latitude-height structure of this prominent DE3 was further investigated using SD/WACCM-X. DE3 amplitudes were found to be largest around the F-layer peak near 200-350 km, with two well-defined enhancements near 15°N and 15°S MLAT associated with the EIA and maxima of $\sim$8x10^4 cm^{-3}. The modeled DE3 temperature amplitudes were found to exhibit largest amplitudes around 110-120 km, in accord with previous modeling and observational results (e.g., Truskowski et al., 2014; Gasperini et al., 2015, 2017a). Departure from a purely equatorially symmetric latitude structure and broadening of latitude structures with height of the thermospheric DE3 was explained in terms of the combined effect of mean winds and dissipation. The vertical wavelength of the modeled temperature DE3 was found to be $\sim$49.8 km indicative of a predominant first symmetric Hough mode.

This study presented first results of the DE3 tide as observed by the NASA-funded SORTIE CubeSat. The results herein provide evidence for the extent to which global-scale tidal activity related to the tropical troposphere can influence the IT system. This study also demonstrates SORTIE and ICON to be excellent observational platforms for studying the influence of terrestrial weather on IT variability. Complementary and concurrent measurements from SORTIE's and ICON's near identical IVM instruments at different altitudes are shown to be particularly valuable.

Acknowledgments

The SORTIE mission is supported from NASA HQ by Grant 80NSSC18K0094 to Atmospheric & Space Technology Research Associates (ASTRA) LLC. ICON is supported by NASAs Explorers Program through contracts NNG12FA45C and NNG12FA42I. ASTRA is grateful for support from U.C. Berkeley and the ICON mission via Subcontract No: 00008210. ICON IVM-A data products (Level 2.7, Version 4) are publicly available at $ftp://icon-science.ssl.berkeley.edu/pub$. Post-processed SORTIE IVM Level 2 ion density data can be accessed on Zenodo at doi:10.5281/zenodo.4589362. TIMED/SABER temperatures (version v2.0) can be freely accessed at $http://saber.gats-inc.com/$. WACCM-X history files can be accessed at the NCAR/CDG (https://doi.org/10.26024/5b58-nc53) and are archived on the NCAR/HAO Campaign Space. Further information on the ICON IVM data used in this study can be found at: $ftp://icon-science.ssl.berkeley.edu/$.

References

Appleton, E. V. (1946), Two anomalies in the ionosphere, Nature, 157, 691.

Balan, N., and G. J. Bailey (1995), Equatorial plasma fountain and its effects: Possibility of an additional layer, J. Geophys. Res., 100, 21421-21432, doi:10.1029/95JA01555.

Chang, L. C., Lin, C.H., Liu, J.Y., Balan, N., Yue, J., and Lin, J.T. (2013), Seasonal and local time variation of ionospheric migrating tides in 2007-2011 FORMOSAT3/COSMIC and TIEGCM total electron content, J. Geophys. Res. Space Physics, 118, 2545-2564, doi:10.1002/jgra.50268.

Chapman, S., and R. S. Lindzen (1970), Atmospheric Tides, Springer, New York.

Cho, Y.-M., and G. Shepherd (2015), Resolving daily wave 4 nonmigrating tidal winds at equatorial and midlatitudes with WINDII: DE3 and SE2, J. Geophys. Res. Space Physics, 120, 10,05310,068, doi:10.1002/ 2015JA021903.

Crowley, G., C. Fish, M. Pilinski, E. Stromberg et al. (2016), Scintillation Observations and Response of The Ionosphere to Electrodynamics (SORTIE), Proceedings of the 30th Annual AIAA/USU SmallSat Conference, paper: SSC16-VI-3.

Fang, T.-W., H. Kil, G. Millward, A. D. Richmond, J.-Y. Liu, and S.-J. Oh (2009), Causal link of the wave-4 structures in plasma density and vertical plasma drift in the low-latitude ionosphere, J. Geophys. Res., 114, A10315, doi:10.1029/2009JA014460.

Forbes, J. M. (2000), Wave coupling between the lower and upper atmosphere: Case study of an ultra-fast Kelvin wave, J. Atmos. Terr. Phys, 62, 1603-1621.

Garcia-Comas, M., et al. (2008), Errors in SABER kinetic temperature caused by non-LTE model parameters, J. Geophys. Res., 113, D24, doi: 10.1029/2008JD010105.

Gasperini, F., J. M. Forbes, E. N. Doornbos, and S. L. Bruinsma (2015), Wave coupling between the lower and middle thermosphere as viewed from TIMED and GOCE, J. Geophys. Res., 120, 5788-5804, doi:10.1002/2015JA021300.

Gasperini, F., Forbes, J. M., and Hagan, M. E. (2017a), Wave coupling from the lower to the middle thermosphere: Effects of mean winds and dissipation, J. Geophys. Res., 122, 7781-7797, doi:10.1002/2017JA024317.

Gasperini, F, M. E. Hagan, and Y. Zhao (2017b), Evidence of tropospheric 90-day oscillations in the thermosphere, Geophys. Res. Lett., doi:10.1002/2017GL075445.

Gasperini, F., Forbes, J. M., Doornbos, E. N., and Bruinsma, S. L. (2018), Kelvin wave coupling from TIMED and GOCE: Inter/intra-annual variability and solar activity effects, J. Atmos. Sol.-Terr. Phys., 171, 176-187, doi:10.1016/j.jastp.2017.08.034.

Gasperini, F., Liu, H., and McInerney, J. (2020), Preliminary evidence of Madden-Julian Oscillation effects on ultrafast tropical waves in the thermosphere, J. Geophys. Res., 125, e2019JA027649, doi:10.1029/2019JA027649.

Gelaro, R., McCarty, W., Suarez, M. J., Todling, R., Molod, A., Takacs, L., et al. (2017), The modern-era retrospective analysis for research and applications, version 2 (MERRA-2), J. Climate, 30, 5419-5454, doi:10.1175/JCLI-D-16-0758.1.

Hagan, M. E. and J. M. Forbes (2002), Migrating and nonmigrating diurnal tides in the middle and upper atmosphere excited by tropospheric latent heat release, J. Geophys. Res., 107(D24), 4754, doi: 10.1029/2001JD001236.

Hagan, M.E., A. Maute, R.G. Roble, A.D. Richmond, T.J. Immel, and S.L. England (2007), Connections between deep tropical clouds and the Earths ionosphere, Geophys. Res. Lett., 34, L20109, doi:10.1029/2007GL030142.

Hagan, M. E. (1996), Comparative effects of migrating solar sources on tidal signatures in the middle and upper atmosphere, J. Geophys. Res., 101, 21213-21222.

He, M., L. Liu, W. Wan, and Y. Wei (2011), Strong evidence for couplings between the ionospheric wave4 structure and atmospheric tides, Geophys. Res. Lett., 38, L14101, doi:10.1029/2011GL047855.

Heelis, R. A., Lowell, J. K., and Spiro, R. W. (1982), A model of the high-latitude ionospheric convection pattern, J. Res. Lett., 87, 63390-6345.

Heelis, R.A., Stoneback, R.A., Perdue, M.D., Depew, M.D., Morgan, W.A., Mankey, M.W., Lippincott, C.R., Harmon, L.L., and Holt, B.J., (2017), Ion Velocity Measurements for the Ionospheric Connections Explorer, Sp. Sci. Rev., 212(1-2), 615-629, doi:10.1007/s11214-017-0383-3.

Hurrell, J. W., Holland, M. M., Gent, P. R., Ghan, S., Kay, J. E., Kushner, P. J., et al. (2013), The community earth system model: A framework for collaborative research, Bull. of the Am. Met. Soc., 94(9), 1339-1360, doi:10.1175/BAMS-D-12-00121.1.

Immel, T. J., E. Sagawa, S. L. England, S. B. Henderson, M. E. Hagan, S. B. Mende, H. U. Frey, C. M. Swenson, and L. J. Paxton (2006), The control of equatorial ionospheric morphology by atmospheric tides, Geophys. Res. Lett., 33 (15), doi:10.1029/2006GL026161.

Immel, T.J., England, S.L., Mende, S.B. et al, (2018), The Ionospheric Connection Explorer Mission: Mission Goals and Design, Sp. Sci. Rev. 214, 13, doi:10.1007/s11214-017-0449-2.

Jin, H., Y. Miyoshi, H. Fujiwara, and H. Shinagawa (2008), Electrodynamics of the formation of ionospheric wave number 4 longitudinal structure, J. Geophys. Res., 113, A09307, doi:10.1029/2008JA013301.

Lei, J., J.P. Thayer, W. Wang, J. Yue, and X. Dou (2014), Nonmigrating tidal modulation of the equatorial thermosphere and ionosphere anomaly, J. Geophys. Res., 119, 30363043, doi:10.1002/2013JA019749.

Lieberman, R. S., Riggin, D. M., Ortland, D. A., Nesbitt, S. W., and Vincent, R. A. (2007), Variability of mesospheric diurnal tides and tropospheric diurnal heating during 1997-1998, J. Geophys. Res., 112, D20110, doi:10.1029/2007JD008578.

Lieberman, R. S. (1991), Nonmigrating diurnal tides in the equatorial middle atmosphere, J. Atmos. Sci., 48, 1112 - 1123.

Lin, C.H., C.C. Hsiao, J.Y. Liu, and C.H. Liu (2007), Longitudinal structure of the equatorial ionosphere: Time evolution of the four-peaked EIA structure, J. Geophys. Res., 112, A12305, doi:10.1029/2007JA012455.

Liu, H., and S. Watanabe (2008), Seasonal variation of the longitudinal structure of the equatorial ionosphere: Does it reflect tidal influences from below?, J. Geophys. Res., 113, A08315, doi:10.1029/2008JA013027.

Liu, H., M. Yamamoto, and H. Luhr (2009), Wave-4 pattern of the equatorial mass density anomaly: A thermosphere signature of tropical deep convection, Geophys. Res. Lett., 36, L18104, doi:10.1029/2009GL039865.

Liu, H. -L. (2016), Variability and predictability of the space environment as related to lower atmosphere forcing, Space Weather, 14, 634-658, doi:10.1002/2016SW001450.

Liu, J., Liu, H., Wang, W., Burns, A. G., Wu, Q., Gan, Q., et al. (2018), First results from the ionospheric extension of WACCM-X during the deep solar minimum year of 2008, J. Geophys. Res., 123, 1534-1553, doi:10.1002/2017JA025010.

Maute, A., A. D. Richmond, and R. G. Roble, Sources of low-latitude ionospheric E x B drifts and their variability (2012), J. Geophys. Res., 117, A06312, doi:10.1029/2011JA017502.

Mertens Christopher J., M Martin G. Mlynczak, Manuel Lpez-Puertas, Peter P. Wintersteiner, R. H. Picard, Jeremy R.Winick, Larry L.Gordley, and James M.Russell III (2001), Retrieval of mesospheric and lower thermospheric kinetic temperature from measurements of CO_2 15 μm Earth limb emission under non-LTE conditions, Geophys. Res. Lett., 28, 1391-1394.

Mukhtarov, P., and D. Pancheva (2011), Global ionospheric response to nonmigrating DE3 and DE2 tides forced from below, J. Geophys. Res., 116, A05323, doi:10.1029/2010JA016099.

Oberheide, J., J. M. Forbes, X. Zhang, and S. L. Bruinsma (2011), Wavedriven variability in the ionosphere thermospheremesosphere system from TIMED observations: What contributes to the wave 4?, J. Geophys. Res., 116, A01306, doi:10.1029/2010JA015911.

Oberheide, J., J. Forbes, K. Hausler, Q. Wu, and S. L. Bruinsma (2009), Tropospheric tides from 80400 km: Propagation, inter-annual variabil- ity and solar cycle effects, J. Geophys. Res., doi:10.1029/2009JD012388.

Oberheide, J., Hagan, M. E., Ward, W. E., Riese, M., and Offermann, D. (2000), Modeling the diurnal tide for the Cryogenic Infrared Spectrometers and Telescopes for the Atmosphere (CRISTA) 1 time period, J. Geophys. Res., 105(A11), 24917-24929, doi:10.1029/2000JA000047.

Onohara, A. N., Batista, I. S., and Batista, P. P. (2018), Wavenumber4 structures observed in the lowlatitude ionosphere during low and high solar activity periods using FORMOSAT/COSMIC observations, Ann. Geophy., 36(2), 459-471, doi:10.5194/angeo-36-459-2018.

Ren, Z., W. Wan, L. Liu, and J. Xiong (2009), Intra-annual variation of wave number 4 structure of vertical E B drifts in the equatorial ionosphere seen from ROCSAT-1, J. Geophys. Res., 114, A05308, doi:10.1029/2009JA014060.

Sagawa, E., T. J. Immel, H. U. Frey, and S. B. Mende (2005), Longitudinal structure of the equatorial anomaly in the nighttime ionosphere observed by IM-

AGE/FUV, J. Geophys. Res., 110, A11302, doi:10.1029/ 2004JA010848.

Truskowski, A.O., Forbes, J.M., Zhang, X., and S.E. Palo (2014), New perspectives on thermosphere tides - 1. Lower thermosphere spectra and seasonal-latitudinal structures, Earth, Planets and Space, 66-136, doi:10.1186/s40623-014-0136-4.

Wan, W., L. Liu, X. Pi, M.-L. Zhang, B. Ning, J. Xiong, and F. Ding (2008), Wavenumber-4 patterns of the total electron content over the low latitude ionosphere, Geophys. Res. Lett., 35, L12104, doi:10.1029/2008GL033755.

Wan, W., J. Xiong, Z. Ren, L. Liu, M.L. Zhang, F. Ding, B. Ning, B. Zhao, and X. Yue (2010), Correlation between the ionospheric WN4 signature and the upper atmospheric DE3 tide, J. Geophys. Res., 115, A11303, doi:10.1029/2010JA015527.

Wan, W., Z. Ren, F. Ding, J. Xiong, L. Liu, B. Ning, B. Zhao, G. Li, M.-L. Zhang (2012), A simulation study for the couplings between DE3 tide and longitudinal WN4 structure in the thermosphere and ionosphere, J. of Atm. and Sol.-Terr. Phy.,, 90-91, 52-60, doi:10.1016/j.jastp.2012.04.011.

Figure 1. (a) Time series of the daily F10.7 solar flux (red curve) and 3-hourly ap (blue curve) during May 27 - June 5, 2020. (b)-(d) Time series of ICON (blue plus signs) and SORTIE (red squares) local solar time at 25°N (panel *b*), equator (panel *c*), and 25°S (panel *d*).

Figure 2. Global latitude (60°S-60°N) versus longitude (180°W-180°E) maps of SORTIE (upper panels) and ICON (lower panels) Ion Velocity Meter (IVM) ion density measured during May 27 - June 5, 2020. SORTIE (ICON) daytime, i.e., ∼10-14 LT (∼14-18 LT), averages are shown in panel a (panel b); while SORTIE (ICON) nighttime, i.e., ∼22-2 LT (∼2-6 LT) averages are shown in panel a' (b'). Panels a'' and b'' show maps of half ascending and descending node differences (i.e., daytime-nighttime differences). The black dots in panels a-a' and b-b' show the measurement locations. ICON ion density is scaled (multiplied) by a factor of 2 given ICON's higher mean altitude (∼575-610 km) compared to SORTIE (∼418-427 km). This scaling is performed to use the same color bar for both ICON and SORTIE.

Figure 3. Period versus zonal wavenumber amplitude spectra of SORTIE IVM ion density at MLAT 40°N (panel a), 10°S-10°N (panel a'), 40°S (panel a'') during May 27 - June 25, 2020, and of SD/WACCM-X ion density at MLAT 40°N (panel b), 10°S-10°N (panel b'), 40°S (panel b'') during May 27 - June 5, 2020. Note that this 10-day window for WACCM-X is adopted for consistency with the SORTIE and ICON results shown in Figure 2. Panels a' and b' show the same results as in panels a and b, but with the migrating tide set to zero. Eastward propagating waves are shown with negative values. The diurnal s=-3 DE3 is clearly seen in both the SORTIE and SD/WACCM-X low-latitude ionosphere spectra, along with a large DW1.

Figure 4. (a) MLAT versus zonal wavenumber diurnal amplitude spectra of SORTIE IVM ion density during May 27 - June 25, 2020. (b) Same as (a) but using SD/WACCM-X output during May 27 - June 5, 2020. The prominent ionospheric s=-3 DE3 exhibits amplitudes upward of $3 \mathrm{x} 10^4$ cm^{-3} in both observations (panel a') and the model (panel b').

Figure 5. Time series of SORTIE IVM ion density DE3 amplitudes (panel a) and phases (panel a') derived using least squares fitting within 30-day sliding windows during May 27 - September 15, 2020. The blue vertical boxes identify 1-σ uncertainly estimates in the amplitudes and phases output by the fitting procedure. Panels b-b' show the SD/WACCM-X height ($\sim$100-450 km) versus MLAT (60°S-60°N) ion density DE3 amplitudes and phases, respectively. Panels c-c' show the same results as in panels b-b', but for neutral temperature DE3. The vertical wavelength of the modeled temperature DE3 inferred from its vertical phase progression (panel c') is $\sim$49.8 km, consistent with a predominant first symmetric Hough mode.

Figure 6. Latitude (60°S-60°N) versus longitude (180°W-180°E) maps of TIMED/SABER kinetic temperatures near 105 km during May 27 - June 5, 2020 at the descending node (panel *a*) near 3-5 LT, ascending node (panel *b*) near 15-17 LT, and their half difference (panel *c*). A prominent longitudinal WN4 structure is evident in the differences (panel *c*) consistent with the concurrent ionospheric DE3 signature observed by SORTIE (ICON) IVM near 420 km (590 km).

Figure 1.

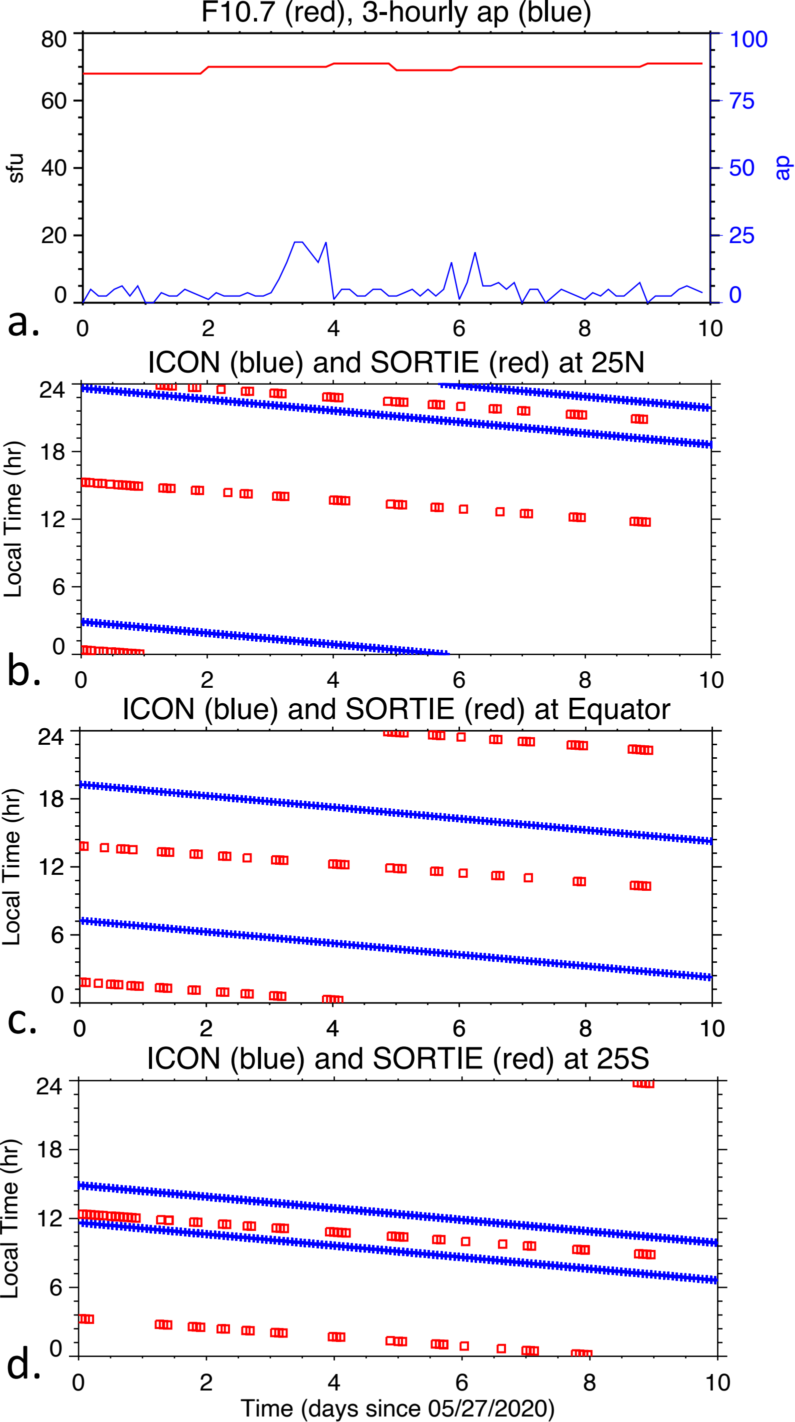

F10.7 (red), 3-hourly ap (blue)
sfu
ap
a.
ICON (blue) and SORTIE (red) at 25N
Local Time (hr)
b.
ICON (blue) and SORTIE (red) at Equator
Local Time (hr)
c.
ICON (blue) and SORTIE (red) at 25S
Local Time (hr)
d.
Time (days since 05/27/2020)

Figure 2.

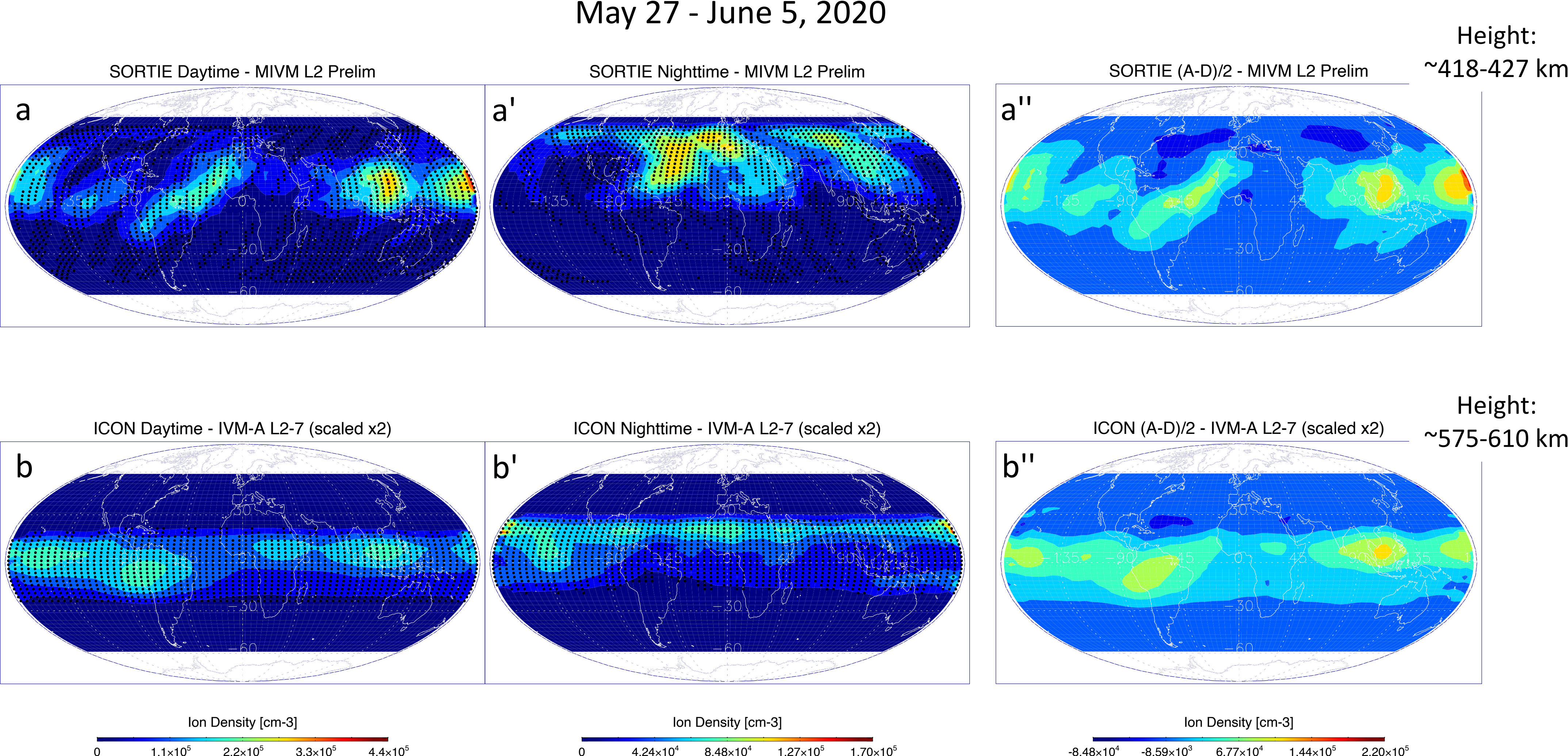
May 27 - June 5, 2020
Height: ~418-427 km
SORTIE Daytime - MIVM L2 Prelim
SORTIE Nighttime - MIVM L2 Prelim
SORTIE (A-D)/2 - MIVM L2 Prelim
a
a'
a''
Height: ~575-610 km
ICON Daytime - IVM-A L2-7 (scaled x2)
ICON Nighttime - IVM-A L2-7 (scaled x2)
ICON (A-D)/2 - IVM-A L2-7 (scaled x2)
b
b'
b''
Ion Density [cm-3]
0 1.1x10^5 2.2x10^5 3.3x10^5 4.4x10^5
Ion Density [cm-3]
0 4.24x10^4 8.48x10^4 1.27x10^5 1.70x10^5
Ion Density [cm-3]
-8.48x10^4 -8.59x10^3 6.77x10^4 1.44x10^5 2.20x10^5

Figure 3.

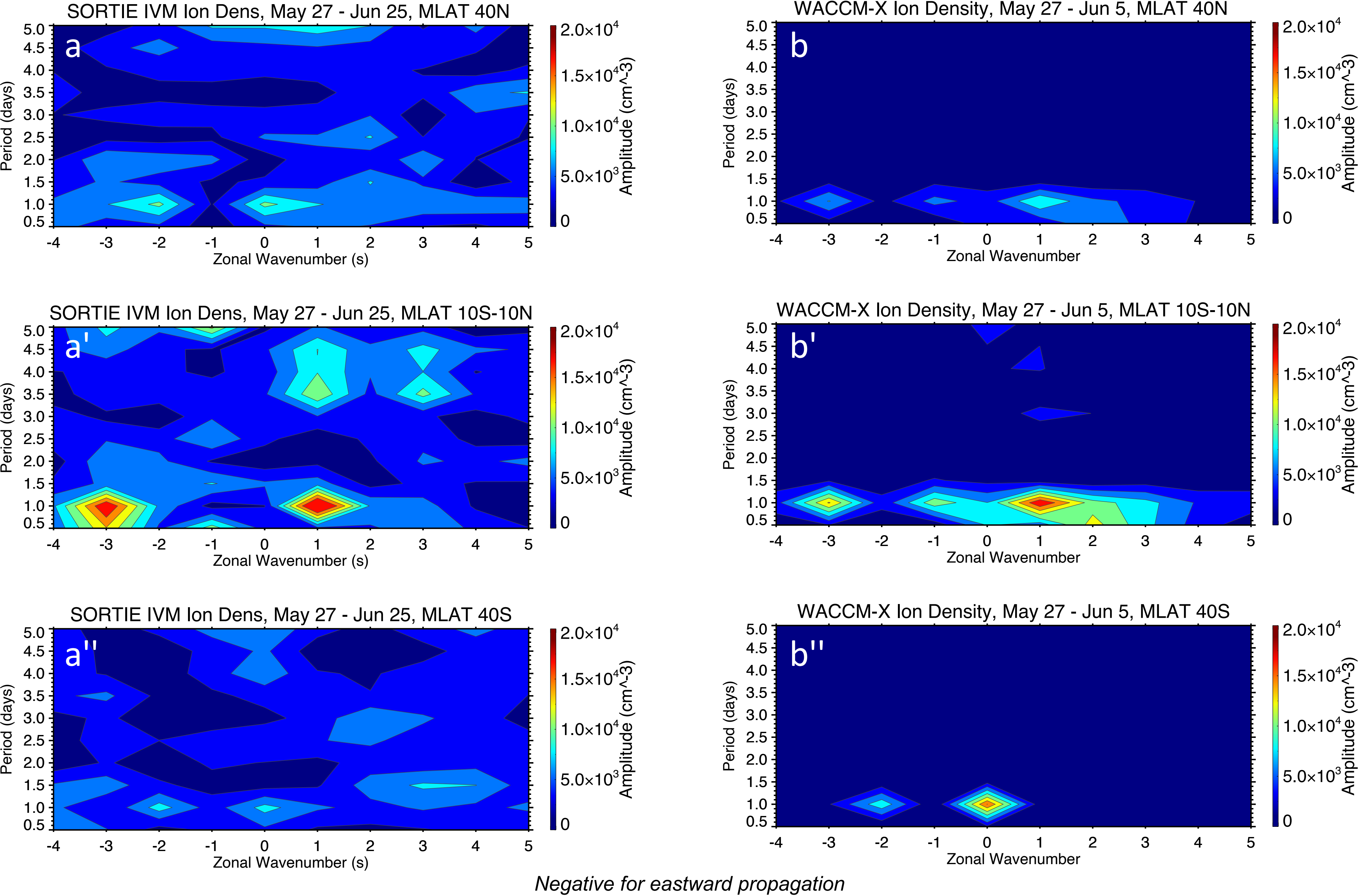

SORTIE IVM Ion Dens, May 27 - Jun 25, MLAT 40N
a
WACCM-X Ion Density, May 27 - Jun 5, MLAT 40N
b
SORTIE IVM Ion Dens, May 27 - Jun 25, MLAT 10S-10N
a'
WACCM-X Ion Density, May 27 - Jun 5, MLAT 10S-10N
b'
SORTIE IVM Ion Dens, May 27 - Jun 25, MLAT 40S
a''
WACCM-X Ion Density, May 27 - Jun 5, MLAT 40S
b''
Period (days)
Zonal Wavenumber (s)
Zonal Wavenumber
Amplitude (cm^-3)
2.0×10^4
1.5×10^4
1.0×10^4
5.0×10^3
0
Negative for eastward propagation

Figure 4.

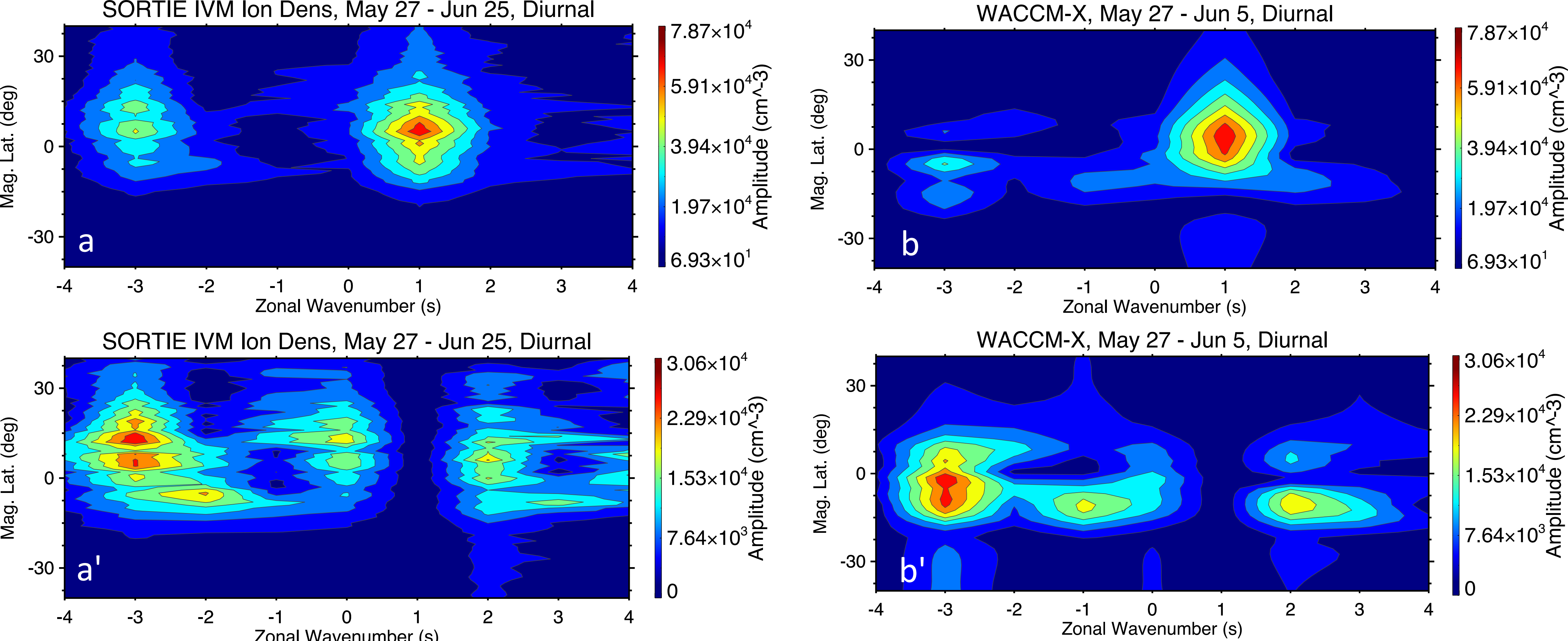

Negative for eastward propagation

Figure 5.

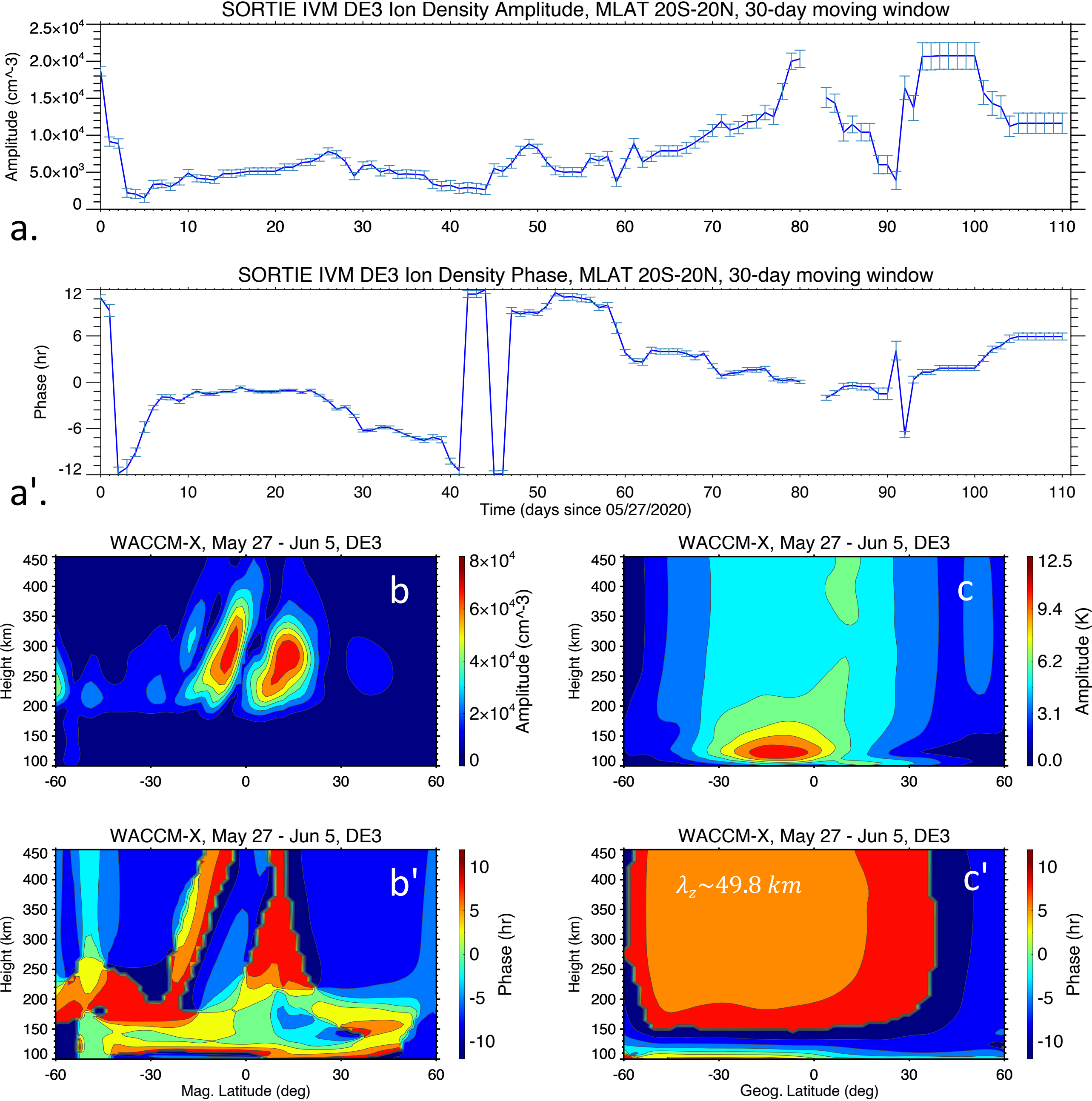
SORTIE IVM DE3 Ion Density Amplitude, MLAT 20S-20N, 30-day moving window
Amplitude (cm^-3)
a.
SORTIE IVM DE3 Ion Density Phase, MLAT 20S-20N, 30-day moving window
Phase (hr)
a'.
Time (days since 05/27/2020)
WACCM-X, May 27 - Jun 5, DE3
b
Amplitude (cm^-3)
c
Amplitude (K)
b'
Phase (hr)
c'
λ_z~49.8 km
Height (km)
Mag. Latitude (deg)
Geog. Latitude (deg)

Figure 6.

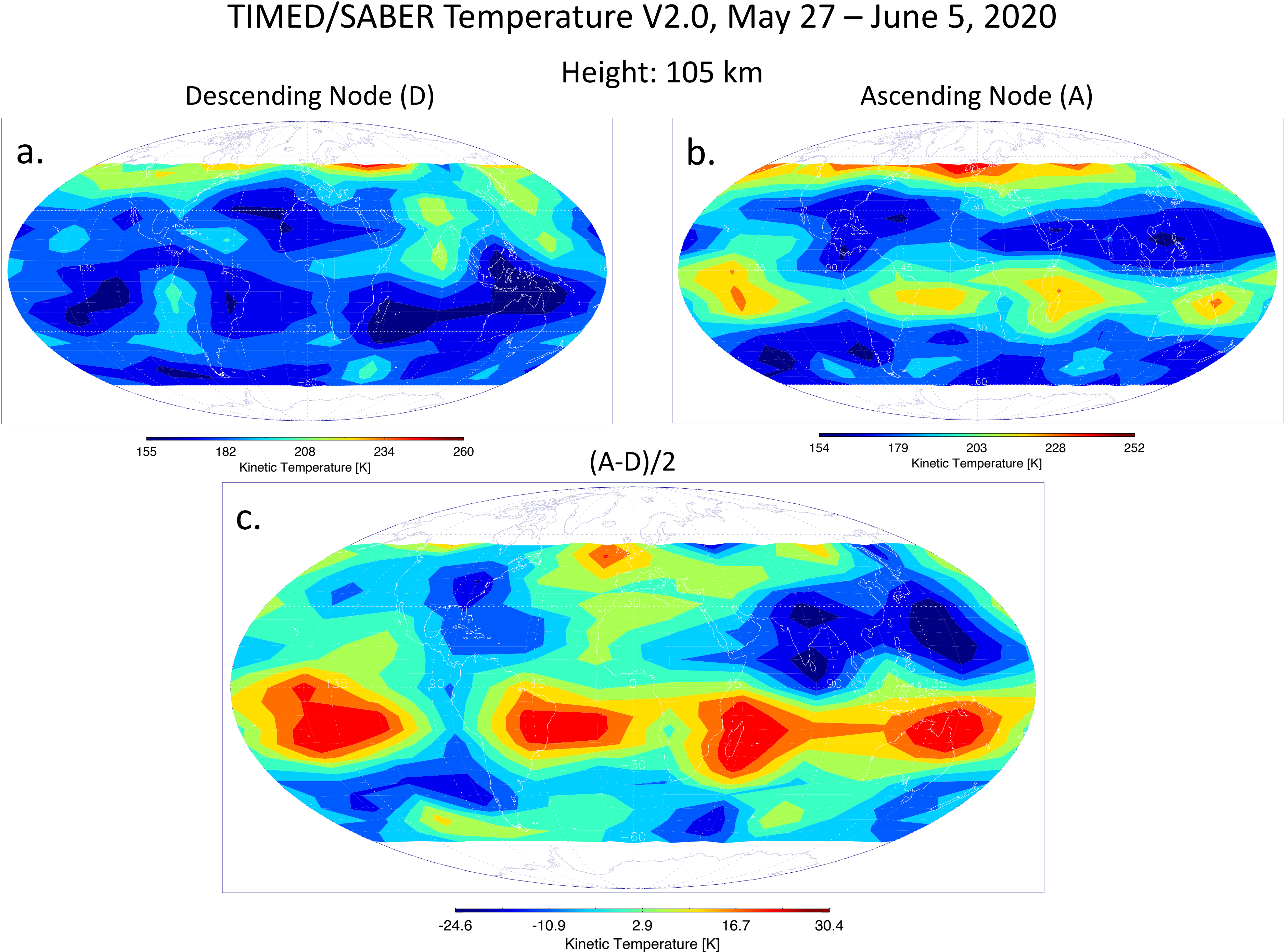
TIMED/SABER Temperature V2.0, May 27 – June 5, 2020
Height: 105 km
Descending Node (D)
Ascending Node (A)
a.
b.
155
182
208
234
260
Kinetic Temperature [K]
154
179
203
228
252
Kinetic Temperature [K]
(A-D)/2
c.
-24.6
-10.9
2.9
16.7
30.4
Kinetic Temperature [K]